Experimental band structure of cadmium sulfide

N. G. Stoffel
Department of Physics, University of Wisconsin, Madison, Wisconsin 53706
(Received 7 April 1983)

We have investigated the bulk electronic structure of wurtzite CdS using angle-resolved photoelectron spectroscopy with synchrotron radiation. We find that direct transitions largely determine the shape of the experimental spectra. Information from all high-symmetry points in the Brillouin zone is available from normal- and off-normal-emission spectra with the aid of polarization selection rules. A comparison with our experimentally determined critical-point energies shows that existing theoretical band-structure calculations for wurtzite CdS are qualitatively correct, but underestimate the extent of the band dispersion. For example, we observe an upper-valence-band width of 4.5 eV, which is significantly larger than the predicted values of 2.7—3.3 eV. Our spectra also reveal fine structure in the Cd 4*d* core-level spectra. This suggests that the Cd 4*d* electrons are involved in the chemical bonding.

I. INTRODUCTION

Cadmium sulfide is by far the most extensively studied compound in the II-VI family.[1] Renewed interest in its electronic properties has been generated by the possibility of using CdS in thin-film heterojunction solar cells. The valence- and conduction-band edges have been examined with optical spectroscopy,[2,3] while excitonic states[4] and a variety of defect states in the band gap have been studied by luminescence spectroscopy. As a result, the intrinsic electronic states near the 2.5-eV fundamental gap and many of the extrinsic defect states in the gap are believed to be well understood.

In contrast, the electronic structure is less well characterized away from the band gap, and fundamental questions about the extended electronic structure of CdS remain unanswered. Compared to the III-V compounds, for which band structures have been calculated over a wide energy range,[5,6] the II-IV compounds have been the subject of relatively little theoretical attention. This is particularly true of the II-IV compounds, which crystallize in the wurtzite polymorph, as does CdS. In fact, the most recent calculations of the electronic structure of CdS (Refs. 7—9) have been undertaken for the simpler zinc-blende structure, rather than for the technologically more important[10] wurtzite polymorph. Both structures are tetrahedrally coordinated, but the wurtzite unit cell contains four atoms as compared to two for the zinc blende. The resulting doubling of the number of states in the valence band, the lower symmetry of the hexagonal lattice, the higher ionicity, and the presence of *d* bands within the valence bands, all contribute to the complexity of calculations of the electronic structure of wurtzite CdS, compared to zinc-blende III-V compounds.

Optical spectroscopy can provide information about the extended band structure. However, two inherent drawbacks to this approach for band-structure determination are that it only provides information about a limited number of points in reciprocal space, and it only yields relative energies of bands. Several ultraviolet reflectivity measurements have been conducted on CdS.[2,3] However, the complexity of the wurtzite band structure and the inadequacy of the theoretical descriptions of CdS made the interpretation of the reflectivity data very difficult. There is no agreement in the reflectivity literature[2,3,11] concerning the origins of the transitions above photon energies of 5 eV. While the optical data did give reliable information about the magnitude of the fundamental band gap and the position of one conduction-band critical point relative to the valence-band maximum, other assignments of critical points in the reflectivity literature were apparently in error. This was demonstrated in subsequent angle-integrated photoemission experiments[12—15] which showed that the valence bands of CdS are wider than implied by the original interpretations of the optical data. Angle-resolved photoelectron spectroscopy (ARPES) provides an even more precise probe of electronic structure.[16] ARPES provides information about both wave vectors and energies of the states involved in optical transitions. It also allows one to selectively study particular points in reciprocal space.

For some zinc-blende III-V compounds the complete valance bands have been mapped out in detail using ARPES.[17,18] The close agreement of theory[5,6] and experiment for these materials indicates that the electronic structures of III-V compounds are well understood. In contrast, no II-VI—compound or wurtzite-compound valence bands have previously been mapped experimentally.[19] The higher multiplicity of bands and the lower symmetry make the complete experimental determination of valence bands more difficult for wurtzite CdS than for zinc-blende compounds. This difficulty is compounded by the lack of reliable calculations of the conduction-band dispersions to guide the interpretation of the experimental data. However, by using angle-resolved photoelectron spectroscopy we are able to determine the valence-band energies for most of the high-symmetry points in CdS. We find large quantitative differences between our mea-

sured widths and critical-point energies for the upper valence band and the currently available theoretical band structures.[20,21] In addition, angle-resolved spectra of the Cd 4*d* levels indicate that the character of these states may be more complicated than was previously supposed.

This paper is organized as follows. Section II describes the experimental procedures. The structure of wurtzite CdS and the theory of band-structure mapping are discussed in Sec. III. Results are presented in Sec. IV along with a discussion of the origin of the photoemission features. In Sec. V we compare the observed critical points with the current theoretical results on the CdS band structure and examine the nature of the final-state dispersions and the role of surface-state emission. The nature of the Cd 4*d* core level and its participation in the chemical bonding are considered in Sec. VI. A summary of our results is given in Sec. VII.

II. EXPERIMENTAL PROCEDURES

These experiments were performed at the University of Wisconsin Synchrotron Radiation Center. Most of the results presented in this paper were obtained using the linearly polarized (7–35)-eV photons from the Seya-Namioka monochromator beamline. Preliminary studies also involved the Brown-Lien "Grasshopper" grazing incidence monochromator beamline (40–90 eV). The electric field vector of the incident photons was always in the plane of the surface, either parallel or perpendicular to the *c* axis of the sample. Experiments were carried out in ultrahigh vacuum (1×10^{-10} Torr). Visually smooth $\{10\bar{1}0\}$ and $\{11\bar{2}0\}$ surfaces were cleaved *in situ* from 3-mm-square bars of single-crystal CdS.[22]

The angle-resolved photoelectron spectra were taken with a plane mirror analyzer (PMA) mounted on a dual-axis goniometer, the design of which is described in detail in Ref. 23. Both polar (θ) and azimuthal (ϕ) angles of detection could be varied independently and read directly with a precision of ±0.5 deg. Because of the freedom of motion afforded by the goniometer, we were also able to perform low-energy electron diffraction (LEED) orientation of the sample using the PMA as the detector.

The combined monochromator and analyzer energy resolution was maintained at 0.5 eV or better for all spectra. The valence-band photoemission peaks exhibited considerable intrinsic broadening. Only the Cd 4*d* levels showed structure that was narrow enough to warrant operation at better than 0.5-eV resolution. The angular acceptance of the PMA was 3°. All results reported in this paper were obtained for at least two different cleaves of each surface. The energy positions of all spectral features reported in this work were quite reproducible, although intensities sometimes varied from cleave to cleave.

The spectra presented in this paper were taken in the constant-final-state energy (CFS) mode of photoemission whereby the photon energy $\hbar\omega$, is swept and the final-state energy window of the detector E_f is held fixed.[24] As is the case for the more conventional energy-distribution curves (EDC's), in the CFS approach the initial-state energy for single-electron excitations $E_i=E_f-\hbar\omega$ may be varied over the occupied states of interest. The CFS technique is more useful than the EDC approach in band-structure studies because the energy, and therefore the momentum, of the detected electrons is the same for every point in a particular spectrum. In particular, this allowed us to take spectra for which the component of electron wave vector parallel to the surface $\vec{k}_{||}$ was a constant, nonzero value, i.e., off-normal emission. This is not possible in the EDC mode of ARPES unless the polar angle of the detector is swept synchronously with energy. All CFS spectra have been normalized to the measured monochromator output.

III. THEORETICAL BACKGROUND

A. Lattice and electronic structure of wurtzite CdS

A perspective illustration of the wurtzite lattice structure appears in Fig. 1, along with the first Brillouin zone and the labeling of the various symmetry elements. The

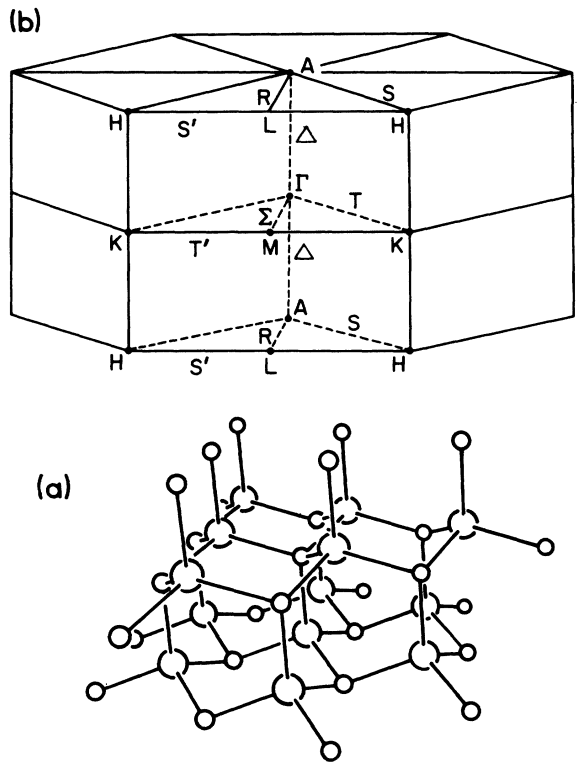

FIG. 1. (a) Perspective view of the wurtzite CdS structure. Hexagonal screw axis $\vec{c}$ runs vertically. Like zinc blende, wurtzite is tetrahedrally coordinated, and is composed of layers of six-membered rings. However, because of the relative orientation of adjacent layers, wurtzite has four atoms per unit cell, rather than two. (b) Conventional labeling of the symmetry elements of the first Brillouin zone is illustrated. Σ and R lines are perpendicular to the $(10\bar{1}0)$ planes in real space, while the T, T', S, and S' line lie perpendicular to the $(11\bar{2}0)$ surface. Any of these lines may, therefore, be probed in a series of photoelectron spectra from the corresponding cleavage surface. This is accomplished by varying the final-state energy to vary $\vec{k}_{\perp}$, while adjusting θ to keep $\vec{k}_{||}$ at the appropriate constant value.

space group is C_{6v}^4 ($P6_3mc$). The lattice constants for CdS are $|\vec{a}|=4.13$ Å and $|\vec{c}|=6.70$Å. The normal to the $\{10\bar{1}0\}$ surfaces is along the $\Gamma\Sigma M$ direction in reciprocal space and lies in a mirror plane of the bulk crystal structure. The normal to the $\{11\bar{2}0\}$ cleavage planes lies in the ΓTK direction and is parallel to one of the glide planes of the wurtzite structure. The reciprocal-lattice vectors have lengths $\vec{A}=1.755$ Å^{-1} and $\vec{C}=0.938$ Å^{-1}. The reciprocal-lattice vector $\vec{C}$ will be referred to in this paper as $\vec{k}_{\Gamma A\Gamma}$, while $\vec{k}_{\Gamma\Delta A}$ refers to the vector equal to one-half of $\vec{k}_{\Gamma A\Gamma}$. Both cleavage faces have primitive 1×1 surface reconstructions. There is no need to consider the double group of the point group C_{6v},[11] since we cannot experimentally resolve the spin-orbit splitting of the valence bands.

In Fig. 2 we present a self-consistent orthogonalized-plane-wave (SCOPW) calculation of the electronic structure of wurtzite CdS done by Euwema *et al.*[20] in 1967, which we have relabeled according to the group notation of Rashba.[25] The states along the Σ and R symmetry lines have a definite parity if relativistic effects are ignored. These bands have been labeled with a "1" to indicate even parity and "2" for odd parity. Bergstresser and Cohen[21] also published a local empirical pseudopotential model (EPM) band structure for CdS in the same year, which differs only slightly with respect to the widths, positions, and topology of the bands. Hereafter, we shall refer to these calculated band structures as ECSD (for Euwema, Collins, Shankland, and DeWitt[20]) and BC (for Bergstresser and Cohen[21]).

Neither of the above studies treats the Cd 4*d* "core levels" in a realistic fashion. These states lie in a narrow band around -9.5 eV. The lower valence band has been observed in x-ray-emission spectroscopy studies[26] at about -12.5 eV, which is 1.5 eV lower than it appears in the calculations of Fig. 2. These states are not detectable in our experiments because they have mostly S 3*s* character, and so they have a negligible cross section for photoexcitation in the uv range.

B. Theory of band-structure mapping

A variety of techniques have been developed for the purpose of determining band dispersions for three-dimensional materials using ARPES. There are a number of reviews[16,27–29] and applications[17–18,30–36] of these methods to which the reader is referred for more information. The method used in this study relies on the three-step model of photoemission,[37] which describes the emission of a photoelectron from a bulk electronic state as the result of three sequential but distinct events. These are (i) the wave-vector-conserving initial optical excitation, (ii) transport of the excited electron to the surface, and (iii) transmission of the photoelectron through the surface.

Each angle-resolved CFS spectrum provides us with the number of electrons photoemitted with a specific direction and energy E_f as a function of photon energy $\hbar\omega$. Direct transitions give rise to peaks in these spectra for which the initial energy is obtained from $E_i=E_f-\hbar\omega$. The difficult task that remains is to ascertain the crystal momentum $\vec{k}_i$ of the corresponding initial state so that points on the energy-band dispersion curves $E_i(\vec{k}_i)$ may be determined. A uv photon carries negligible momentum, so $\vec{k}_i\simeq\vec{k}_f$, and the problem is reduced to finding which final momentum states can result in an external photoelectron with the energy and momentum of an observed peak.

As pointed out by Kane,[38] the component of the wave vector parallel to the surface $\vec{k}_{||}$ will be conserved within a surface reciprocal-lattice vector $\vec{G}$ upon crossing a smooth, ordered surface. If, for the moment, we ignore umklapp processes involving surface $\vec{G}$ vectors, $\hbar\vec{k}_{||}$ of the initial state is given by the projection of the momentum of the detected electron along the surface $\hbar|\vec{k}_{||}|=(2mE_k)^{1/2}\sin\theta$, where E_k is the kinetic energy of the

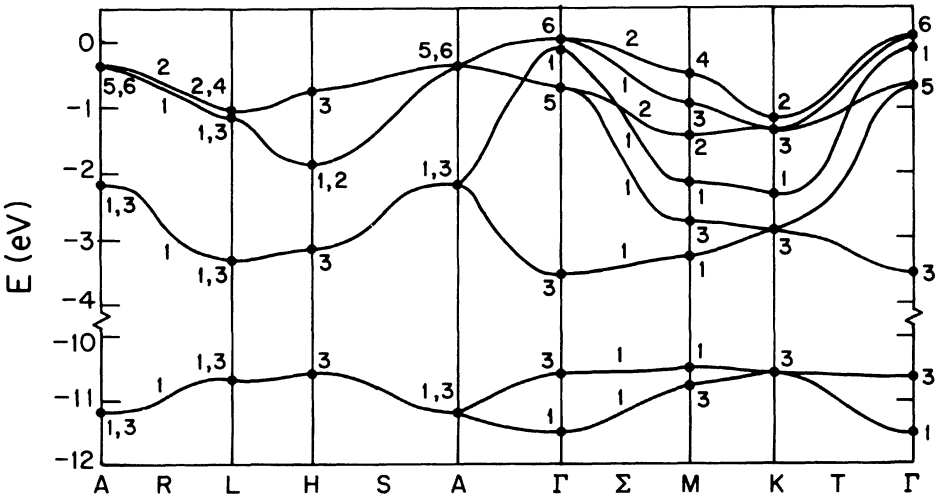

FIG. 2. Calculated self-consistent OPW band structure. Dispersion relationships for the valence bands are presented along symmetry lines as calculated by Euwema *et al.* (Ref. 20). Critical points were calculated using the self-consistent OPW method. Conduction bands were also calculated to an energy of + 9 eV (see Ref. 12). Full width of the valence bands is 3.3 eV. Bergstresser and Cohen (Ref. 21) calculated qualitatively similar bands with 2.7-eV width.

photoelectron and θ is its polar angle of emission. Under these assumptions, we see that the initial-state wave vector can be determined to lie on certain lines in reciprocal space that are normal to the crystal surface. The determination of the normal component of the initial-state wave vector is, therefore, the central problem confronting us if we wish to map the band dispersions. Some knowledge of the final-state dispersion is, in general, essential in order to determine $\vec{k}_\perp$ from the wave vector and E_f of the electron reaching the detector. Most of the previous band-structure studies have been aided by calculated final-state bands. However, no final-state dispersions have as yet been calculated for CdS. Instead, we rely on final-state bands semiempirically determined from our data. We use, as a first approximation, the free-electron-like dispersion $E_f(k)=\hbar^2k^2/2m+E_0$, where E_0 is the free-electron zero of kinetic energy within the crystal. The value of E_0 and corrections to the free-electron bands were then deduced from the data. Angle-resolved studies of metals[30–36] have shown that free-electron-like dispersions provide a reasonably accurate approximation of the final states. This has also been shown to be true for certain III-V semiconductors[17,18] in a sufficiently high energy range, i.e., $E_k > 15$ eV.

For the moment, let us assume that surface umklapp processes are negligible and that the final-state band dispersion is known. Given any known, topologically simple final-state dispersion, $\vec{k}_{||}$ and E_f uniquely specify a value of $\vec{k}_\perp$ *within the extended zone scheme.* The uniqueness of this determination is removed, however, if we consider the possibility of bulk and surface umklapp, which introduces uncertainty about the value of $\vec{k}_{||}$. The probability of umklapp by any one particular $\vec{G}$ vector is small, but scattering by many different $\vec{G}$ vectors is possible at higher energies. In practice, $\vec{k}_\perp$ indeterminacy may be effectively reintroduced by the roughly equal, though small, probability of umklapp by many inequivalent $\vec{G}$ vectors. This may occur even though $\vec{k}_\perp$ is conserved to within a bulk $\vec{G}$ vector for all processes except transfer through the surface.

An additional possibility, which leads to ambiguity in $\vec{k}_\perp$, has been suggested by Grandke *et al.*[39] to explain their ARPES data from PbS. Owing to the presence of the surface, the initial optical excitation need not strictly conserve $\vec{k}_\perp$. If this uncertainty in $\vec{k}_\perp$ is comparable to the size of the Brillouin zone, the ARPES features will be independent of the normal momentum of the detected photoelectrons since all of the $\vec{k}_\perp$ structure is already averaged over the Brillouin zone. Complete three-dimensional band-structure mapping is only possible if the $\vec{k}_\perp$ information is unambiguously preserved. For most of the CdS photoemission features, we find this to be the case. As in other studies,[17,18] however, two types of features are seen in our ARPES spectra: $\vec{k}_\perp$-determined features, which disperse in energy as E_f changes, and $\vec{k}_\perp$-indeterminate emission, which averages over many values of $\vec{k}_\perp$ and tends to emphasize high-density-of-states critical points along $\vec{k}_\perp$. In practice, features resulting from the latter type of emission may be distinguished from the direct, nonumklapped features in that they show no dispersive behavior with photon energy, that is, with $\vec{k}_\perp$.

IV. PRESENTATION OF RESULTS

A. Normal emission from the $(10\bar{1}0)$ surface

We begin with a presentation of the CFS spectra taken in normal emission from the $(10\bar{1}0)$ surface, which are the easiest to interpret. They also illustrate most clearly the procedures followed for the interpretation of the rest of our data. Since the normal to this surface lies in a mirror plane of the crystal, the Hermanson polarization selection rules can be expected to apply.[40] Initial states that are even (odd) with respect to the mirror plane will be excited when the electric field vector $\vec{E}$ of the incident photons is parallel (perpendicular) to this plane. In our geometry this condition is equivalent to $\vec{E}||\vec{c}$ ($\vec{E}\perp\vec{c}$). The initial states that we expect to observe in normal emission from this surface lie along the $\Gamma\Sigma M$ line in $\vec{k}$ space.

Figure 3 shows two series of these CFS spectra. The initial-state energies for these spectra span the upper valence band, but do not include the Cd $4d$ levels at -9.5 eV, which will be discussed separately later. The selection rule for the $\vec{E}\perp\vec{c}$ spectra favor transitions from initial states of Σ_2 symmetry.

Using the calculated bands of ECSD (Fig. 2) as a guide, we can understand the origin of the peaks in Fig. 3(a), which clearly disperse with final-state energy. The degenerate representation Γ_6 at the top of the valence band must split into Σ_1 and Σ_2 representations along the $\Gamma\Sigma M$ line. The Γ_5 representation splits in the same manner. These are the only Σ_2 states in the valence band. Calculations show that both Σ_2 states disperse downward in a roughly parallel fashion as they move towards M. Experimentally we observe two parallel bands that have a maximum energy in the (5—7)-eV CFS spectra. This immediately indicates that the final states in this energy range have Γ-type character. Furthermore, the (16—18)-eV CFS curves contain apparent minima for the dispersion of both bands. Again referring to the calculations, we find that the minimum in the Σ_2 bands occurs at M. The sharp changes in the relative intensity of the two features are additional evidence that the final states, in fact, cross a zone boundary near 17 eV. The wave-function symmetry associated with a band may change discontinuously upon crossing a zone boundary, leading to a change in photoelectric cross sections. These changes in cross section have been used to identify critical-point energies in previous ARPES studies.[41] The uncertainty in the assignment of final-state critical points determined in this manner is fairly large, but the accuracy is sufficient for our purposes. Twelve inequivalent final-state critical points have been identified in our spectra. The kinetic energy and identification of these points are presented in Table I. As explained in the caption, these critical points form a self-consistent picture of the final states as nearly-free-electron-like bands, with $E_0=-8.5$ eV. This is turn allows us to determine the energies of the initial states at

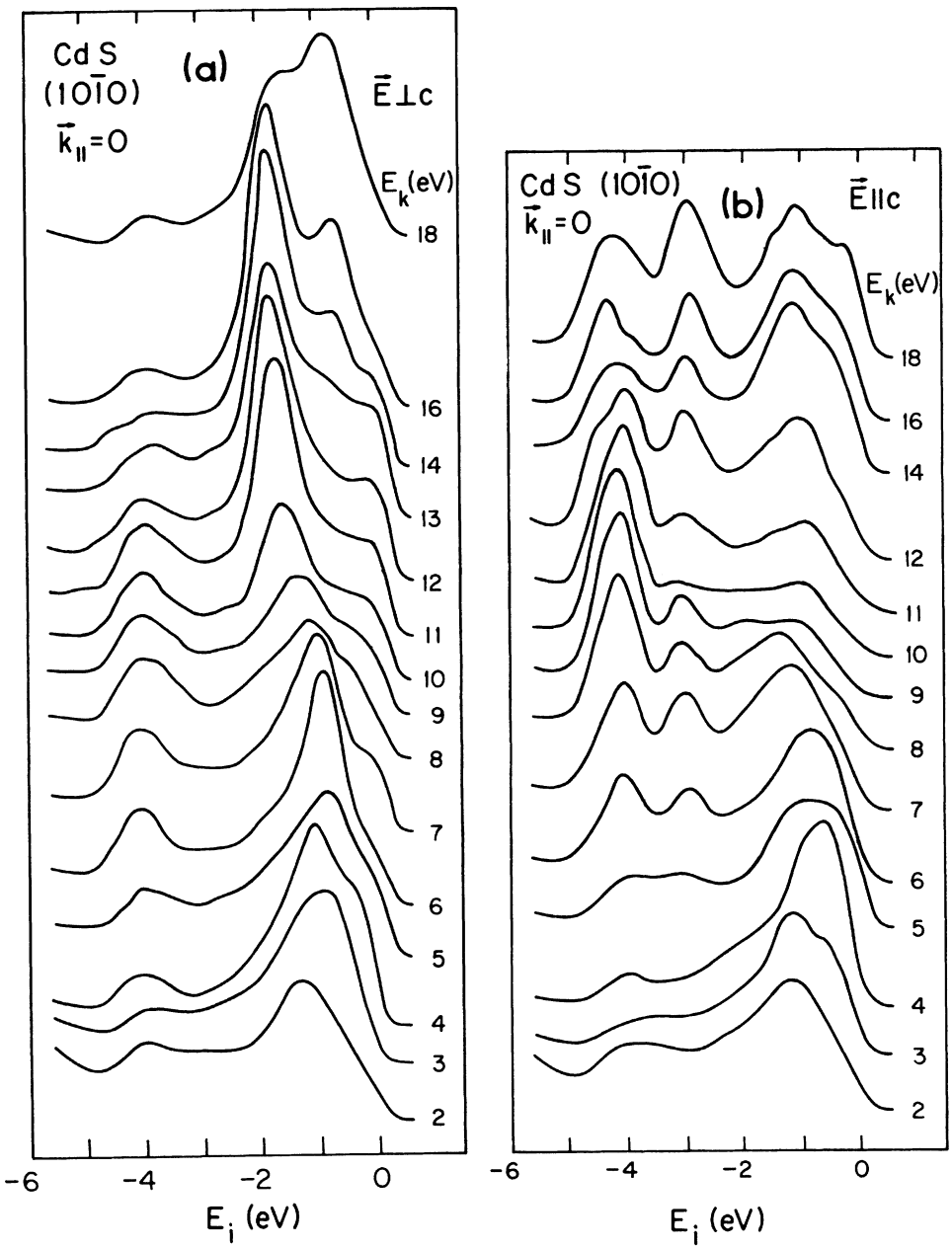

FIG. 3. Series of CFS energy spectra taken in the normal direction of the (10$\bar{1}$0) surface of CdS. Initial states of Σ_2 (odd) symmetry along the Σ line are favored with the $\vec{E}\perp\vec{c}$ photon polarization, while Σ_1 (even) symmetry states are emphasized for $\vec{E}\parallel\vec{c}$. Curves are labeled by their final-state kinetic energy $E_k=E_f-6.65$ eV. Initial-energy scale refers to the position of the valence-band maximum.

most of the high-symmetry points from the CFS spectra. We will comment more on the final states in Sec. V.

We return now to the determination of the valence-band critical points. The strongest feature in all but the uppermost curve in Fig. 3(a) we attribute to the lower Σ_2 state since it reaches a maximum at an energy 0.8 eV below the valence-band maximum. This gives the Γ_5 critical-point energy, -0.8 eV. The peak, which is quite strong in the 18-eV spectrum, is then the upper Σ_2 state. This state is present in varying degrees in most of the spectra with about the same separation between the two Σ_2 peaks. Its maximum position represents the top of the valence band at 0.0 eV. As noted previously, both bands reach their lowest positions in the higher-energy CFS spectra. These minima represent the M_4 critical point at -0.7 eV and the M_2 point at -1.7 eV.

An additional broad dispersionless feature appears in Fig. 3(a) around -4.0 eV. However, all of the bands along the $\Gamma\Sigma M$ line should have Σ_1 symmetry at these energies, and their appearance in the $\vec{E}\perp\vec{c}$ spectra is forbidden by the selection rules outlined above. These emission features occur in the ARPES spectra for all photon ener-

TABLE I. Comparison of the final-state critical-point energies from experiment and from the free-electron model. All energies are in electron volts. E_k is the kinetic energy at which critical-point behavior is observed in our spectra. $\vec{K}$ is the reciprocal-lattice wave vector that we assign to that critical point. Components of the wave vector and the label of the high-symmetry point corresponding to this wave vector are both given. Coordinates are in units of two of the three equiangular reciprocal-lattice vectors $\vec{k}_{\Gamma M\Gamma}$ and the orthogonal $\vec{k}_{\Gamma A\Gamma}$ reciprocal-lattice vector along the hexagonal axis, respectively. E_{fe} is the free-electron energy associated with the corresponding wave vector. Finally, ΔE is the difference between $(E_k - E_0)$ and E_{fe}, where E_0 is taken as -8.5 eV to minimize root-mean-square value of ΔE.

E_k (eV)	$\vec{K}$	E_{fe} (eV)	ΔE (eV)
6±1	$\Gamma(1,0,0)$	11.72	2.78
7±1	$A(1,0,\frac{1}{2})$	12.56	2.94
8±1	$\Gamma(1,0,1)$	12.56	1.43
8±1	$K(\frac{4}{3},\frac{2}{3},0)$	15.62	0.88
8±1	$H(\frac{4}{3},\frac{2}{3},\frac{1}{2})$	16.46	0.04
9±1	$K(\frac{4}{3},\frac{2}{3},1)$	18.97	−1.47
17±1	$M(\frac{3}{2},0,0)$	26.37	−0.87
18±1	$M(\frac{3}{2},0,1)$	29.72	−3.22
20±1	$L(\frac{3}{2},0,\frac{1}{2})$	27.21	1.29
37±4	$\Gamma(2,0,0)$	46.88	−1.38
42±4	$\Gamma(2,0,1)$	50.18	0.32
49±4	$\Gamma(2,0,2)$	60.28	−2.78

gies and polarizations, and at all angles of emission that we have studied. The energy of this feature corresponds closely to the position of a peak in the angle-integrated photoelectron spectra.[12–15] We note that the polarization selection rules are only strictly valid for states on the ΓALM plane. Perpendicularly polarized photons can excite electrons from the lower bands at general points in the zone, but these photoelectrons should not appear in the spectra collected in the mirror plane according to the three-step model. A high density of states is known to occur at −4.0 eV,[12–14] which apparently gives rise to significant emission in the mirror plane through scattering processes.

The polarization of the incident uv photons does have a tremendous effect on the CFS spectra. The normal-emission spectra for $\vec{E}||\vec{c}$ are presented in Fig. 3(b). The differences between these spectra and the results obtained with orthogonal polarization will be explained below in terms of the selection rules. Even without further analysis, though, these results emphasize the importance of taking polarization-dependent spectra. Not only does the polarization dependence allow us to identify the parity of the observed bands, but many of the valence-band peaks would be intrinsically unresolvable in mixed-polarization spectra.

Referring to Fig. 2, we note that there are four Σ_1-type states in the upper valence band between Γ and M, which should be observable in the $\vec{E}||\vec{c}$ polarization. There exists an energy gap along $\Gamma\Sigma M$ that separates the lowest of the Σ_1 states from the other three. This is apparently the source of the valley at −3.5 eV in nearly all the spectra of Fig. 3(b). The calculations indicate that the Γ_3 point corresponds to the lowest energy attained by the lower band, −4.5 eV. This minimum is seen more clearly in Fig. 4(b). The calculations of ECSD show the maximum of the lower Σ_1 band occurring at M_1, but they have not calculated the form of all bands between high-symmetry points. Instead, they often present simple interpolations between calculated critical-point energies. In the pseudopotential calculations of BC, the bands were calculated between symmetry points, and they show the maximum of the band in question occurs between Γ and M. This is in agreement with theoretical results for other wurtzite compounds[42,43] and with our ARPES results. We find that the band reaches a maximum energy of −3.9 eV along the Σ line and then falls to −4.3 eV at M_1.

The minimum observed for the bands above the gap −3.0 eV corresponds to the lower M_3 critical point. Emission at this energy is strongest in the high-energy spectra. This is consistent with the previous identification of these final states with the M point. However, this emission does not move upward in energy as the final-state energy decreases (and $\vec{k}_f$ presumably moves from M toward Γ). We will show that this upward dispersion is observable in off-normal-emission spectra to be presented below.

The peak that is found at −1.1 eV in the upper curves of Fig. 3(b) is assigned to the M_3 critical point in agreement with the calculations that predict that it should fall between M_2 and M_4. There is no clear evidence for the bands connecting this point to Γ_6, however, and the M_1 point emission cannot be identified in any of the spectra.

B. Off-normal emission from the $(10\bar{1}0)$ surface

The spectra gathered in off-normal-emission geometry with $\vec{k}_{||}=k_{\Gamma A\Gamma}$ serve to verify the interpretation of the normal-emission data. In some cases the dispersion is actually clearer in the off-normal spectra than in the normal-emission spectra. The bulk and surface reciprocal-lattice vectors (for both surfaces) along the hexagonal axis are of equal length, 0.938 Å^{-1}. By choosing the polar angle of the PMA appropriately for each spectrum, we can collect only photoelectrons with a wave vector along the $\vec{c}$ axis equal to $\vec{k}_{\Gamma A\Gamma}$. A set of such spectra with $\vec{k}_{||}=\vec{k}_{\Gamma A\Gamma}$ is presented in Fig. 4. The motivation for this choice of $\vec{k}_{||}$ is that, within the reduced-zone scheme, the same initial states are available for this geometry as for normal emission. But the correspondence between spectra in the different collection geometries need not be exact. First, the free-electron model predicts that the final-state wave functions of a given $\vec{k}_{\perp}$ will have different energy for different values of $\vec{k}_{||}$, i.e., different free-electron bands in the reduced zone will be involved.

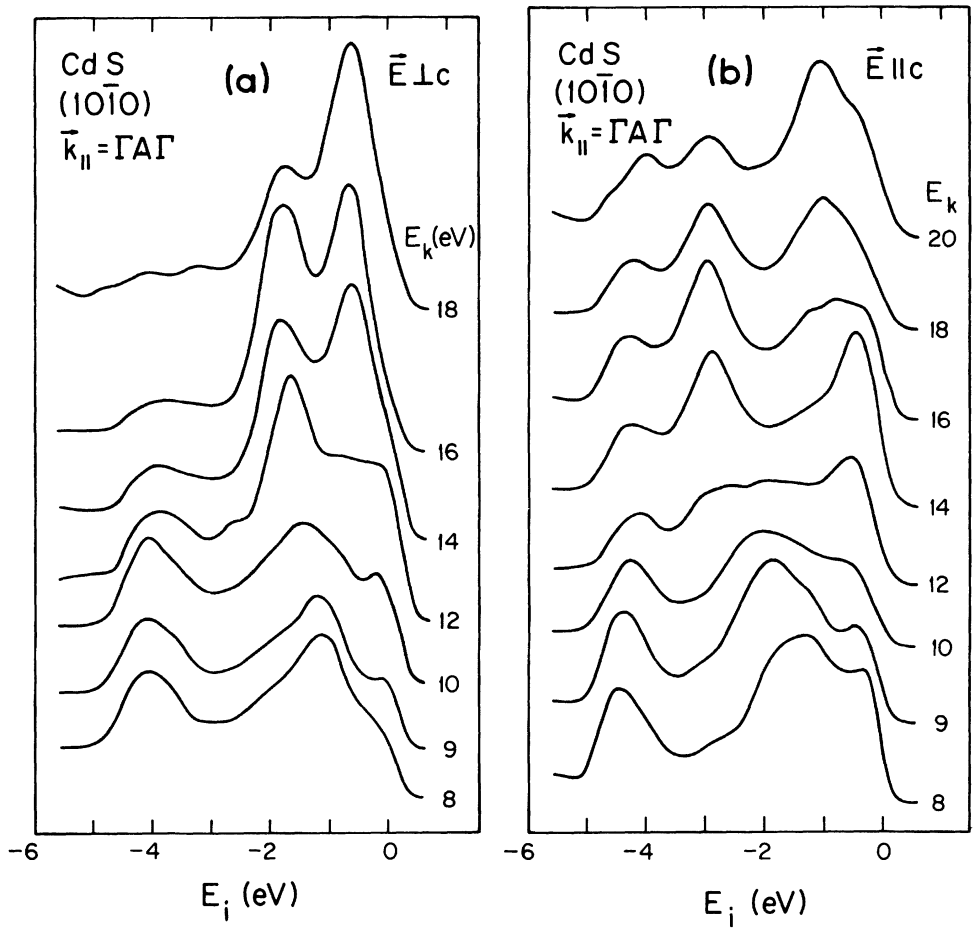

FIG. 4. Off-normal emission spectra from the (10$\bar{1}$0) surface. Angle of detection is chosen for each curve such that $\vec{k}_{||}$ is equal to $\vec{k}_{\Gamma A\Gamma}$, the reciprocal-lattice vector along $\vec{c}$. Emission with this value of $\vec{k}_{\perp}$ originates from the same symmetry line in the reduced Brillouin zone as does the normal emission. Thus the spectra should resemble the spectra of Fig. 3. This conclusion is borne out by a comparison of the data, but the redundant data of this figure provide additional information and resolve some of the ambiguities of the normal-emission data.

Second, while the initial-state eigenvalues must repeat with the periodicity of the Brillouin zone, the transition matrix elements may be quite different for states differing by a reciprocal-lattice vector. Still, as can be seen from a comparison of Figs. 3 and 4, there is an obvious similarity of spectra with $\vec{k}_{||}=0$ and $\vec{k}_{||}=\vec{k}_{\Gamma A\Gamma}$. Constraints imposed by our experimental geometry prevent us from achieving the polar angles required to take spectra with $E_k \leq 8$ eV and $\vec{k}_{||}=\vec{k}_{\Gamma A\Gamma}$. Note that the detection direction remains within the mirror plane of the sample, so the polarization selection rules apply to off-normal spectra along this azimuth. The assignment of the spectral peaks is analogous to that for the normal-emission data. However, we call attention to the following features of the off-normal-emission spectra. Note that the anomalous M_3 emission, which appears in the (6–9)-eV spectra of Fig. 3(b), is absent for the off-normal-emission spectra of Fig. 4(b). Instead the Σ_1 band can clearly be seen dispersing upwards—presumably toward Γ_5 as predicted by group theory. Also, both Σ_2 bands and the minimum of the lowest Σ_1 band can be seen more clearly in the off-normal spectra than in normal emission.

We see that the CFS technique allows us to redundantly probe symmetry lines through off-normal-emission spectra. But more importantly, it gives us access to the states along the *ALH* plane in the Brillouin zone, which cannot be reached by normal emission from any cleavage surface. A series of spectra with $\vec{k}_{||}=\vec{k}_{\Gamma\Delta A}$ appears in Fig. 5. Again the detector remains in the sample mirror plane. The initial states for this data lie on the *ARL* symmetry line. Only five critical points need to be determined along this line due to the extra degeneracy required in the *ALH* plane due to time-reversal symmetry. The uppermost odd and even states R_1 and R_2 are nearly degenerate according to the calculations. It is not surprising that the low-binding-energy features are similar for both polarizations. The highest critical point $A_{5,6}$ should be seen in both polarizations. We take $A_{5,6}$ to be at -0.5 eV, the highest feature in Figs. 5(a) and 5(b). Energies of -1.5 eV for $L_{1,3}$ and -1.4 eV for $L_{2,4}$ are obtained from the lowest excursion of the upper bands of the appropriate polarization.

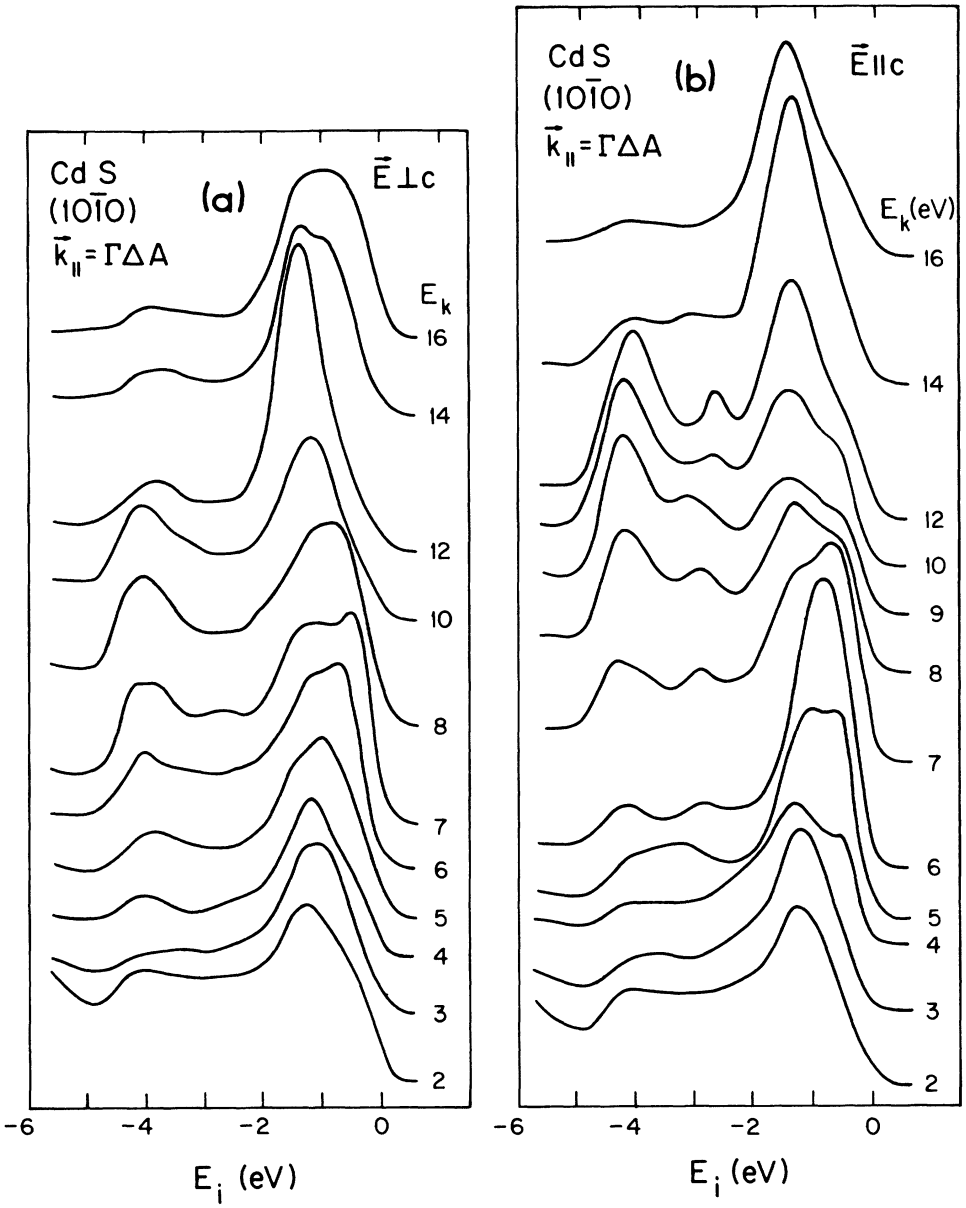

FIG. 5. Spectra with $\vec{k}_{\parallel}$ equal to half a reciprocal-lattice vector along $\vec{c}$. Odd states along the R line in reciprocal space are probed in this geometry with $\vec{E}\perp\vec{c}$, while even states are favored with $\vec{E}\parallel\vec{c}$.

For $\vec{E}\perp\vec{c}$, selection-rule-forbidden emission is seen at -4.0 eV, as it was in normal emission. In contrast, additional dispersive features are seen in this energy range with $\vec{E}\parallel\vec{c}$ as expected. Guided by the calculations, the maximum energy of the polarization-sensitive central features in Fig. 5(b) yields the $A_{1,3}$ point, -2.6 eV. This band reaches a minimum at -4.3 eV, the lower $L_{1,3}$ point.

C. (11$\bar{2}$0) surface results

In order to probe states along the $\Gamma KMLHA$ plane in reciprocal space we must turn to data taken on the (11$\bar{2}$0) surface in the plane of the surface normal and the $\vec{c}$ axis. This is a glide plane of the wurtzite structure, rather than a mirror plane, so no simple polarization selection rules can be applied to the data. Indeed, the spectra taken from the (11$\bar{2}$0) surfaces show much less polarization dependence than the (10$\bar{1}$0) spectra. A presentation of some of the data taken from the (11$\bar{2}$0) surface may be found in Ref. 44, along with an analysis of the data. Results obtained from this surface are included in the next section.

V. COMPARISON WITH THEORY

A. Valence-band critical points

A compilation of the critical points, which have been assigned in preceding sections, is presented in Table II,

TABLE II. Valence-band energies at the high-symmetry points of wurtzite CdS. Energies are in electron volts and the zero of energy is taken as the top of the valence band. Uncertainty is ±0.2 eV unless otherwise indicated. Question marks denote points which cannot be determined from our ARPES results.

Γ_6	0.0	M_4	−0.7	H_3	−1.3
Γ_1	?	M_3	−1.1	$H_{1,2}$	$-2.5^{+0.2}_{-0.4}$
Γ_5	−0.8	M_2	−1.7	H_3	−4.2
Γ_3	−4.5	M_1	?		
		M_3	−3.0	K_2	$-1.4^{+0.2}_{-0.3}$
$L_{2,4}$	−1.4	M_1	−4.3	K_3	?
$L_{1,3}$	−1.5			K_1	−2.8±3
$L_{1,3}$	−4.3	$A_{5,6}$	−0.5	K_3	?
		$A_{1,3}$	−2.6		

along with an estimate of the associated uncertainty. Figure 6 provides a graphical representation of this information along with interpolated bands. We find an overall width of 4.5 eV for the upper valence bands. It has been long known from angle-integrated photoemission experiments that valence-band widths are underestimated by both ECSD (3.3 eV) and BC (2.7 eV). Some of the sources for this error are understood. Eastman *et al.*[12] studied a number of A^NB^{8-N} compounds with angle-integrated photoemission. They found that the local-pseudopotential calculations, which involve fitting to optical data, showed an increasing tendency to underestimate valence-band widths as ionicity increased from group-IV to III-V compounds to II-VI compounds. The inclusion of nonlocal terms in the pseudopotential gives closer agreement with observed widths. The CdS calculations of ECSD, like most early orthogonalized-plane-wave (OPW) calculations, used the Slater exchange parameter $\alpha=1$ because it gave a better fit to the fundamental gap (which was experimentally the best-known quantity at the time). Modern calculations tend to use the Kohn-Sham-Gaspar value $\alpha=\frac{2}{3}$.[45] Use of this value does result in a broader valence band from the SCOPW calculations.[46] Other studies[26,47] have shown that for materials with shallow *d* bands, the width of the valence bands can increase substantially if the *d* states are included in the calculations rather than treated as purely atomic levels. The OPW method gives particularly unsatisfactory results for shallow *d* levels. For instance, ECSD places the Cd 4*d* states about 7 eV below their observed position.

B. Final-state bands

As mentioned above, the determination of the initial-state bands and critical points requires some knowledge of the final-state dispersions. The calculated valence bands and the lowest conduction bands of CdS, which have been calculated up to 7 eV above the conduction-band minimum,[20,21] do not bear any strong resemblance to the free-electron dispersions. Yet, only 5—10 eV above the cutoff of the calculations, where we can directly probe the final states, we observe nearly-free-electron-like dispersions. In this section, we will discuss this surprising result in light of recent theoretical and experimental work on

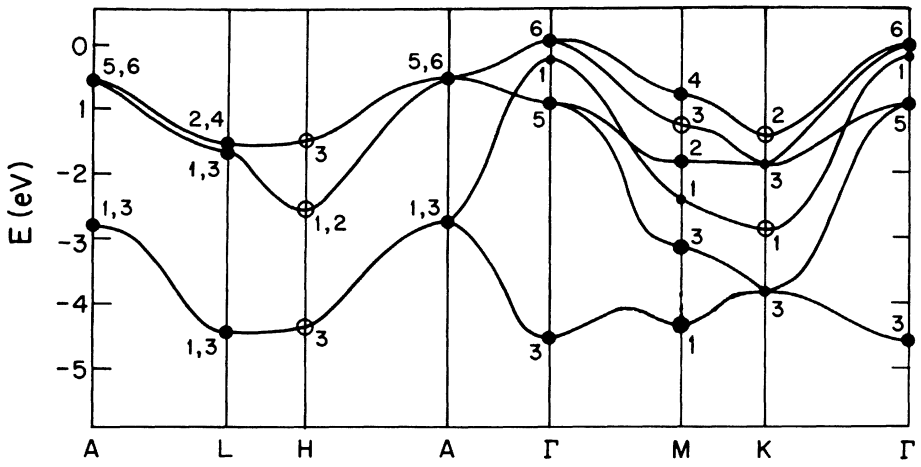

FIG. 6. Experimentally determined energies at high-symmetry points. Numerical values and uncertainties for the critical points are given in Table II. The bands have been interpolated between experimentally determined points using the calculated band structures and our experimental results as a guide.

ARPES. We will show how realistic calculations of the final-state bands give more nearly-free-electron-like dispersions, and explain why the photoemission process, by its very nature, emphasizes the free-electron aspects of those dispersions.

In our work, we find that it is most appropriate to use the extended-zone representation of reciprocal space to determine which final-state wave vectors are important in an observed transition. As mentioned earlier, this representation gives an unambiguous determination of $\vec{k}_\perp$ if E_f, $\vec{k}_{||}$, and the final-state dispersions are known. In contrast, if we fold the free-electron bands into the reduced zone, we find that there are many bands along a line of constant $\vec{k}_{||}$ at any given E_f. Note that the extended-zone scheme puts less emphasis on the internal periodic structure of the crystal potential. In fact, the free-electron bands in extended-zone scheme give the same spherical constant-energy surface in k space as would result if the crystal potential were replaced by a smooth-bottomed well of depth E_0.

Mahan[48] discussed such a model crystal potential with the surface represented by an uncorrugated step in connection with his theory of photoemission from simple metals. Owing to rather complete screening of the atomic cores, this is a reasonably accurate description of the effective potential in these materials. If $\vec{K}=\vec{K}_{||}+\vec{K}_\perp$ is the wave vector of a final state within the crystal, the wave function would have the simple spatial dependence $e^{-i\vec{K}\cdot\vec{r}}$. This wave has a well-defined wave vector parallel to the surface. If this wave is to be transmitted across the edge of the potential well, it can only couple to an external wave function of the form $e^{i\vec{K}_{||}\cdot\vec{r}}$, times a function of z, the perpendicular spatial coordinate. Note that matching of $\vec{K}_{||}$ *in the extended zone* is the important criterion for the transmission of the wave. Mahan termed photoemission occurring through the wave component given above "primary-cone emission." He also recognized that in a real crystal the various Fourier components of the periodic crystal potential mix in other components with the free-electron wave. As a consequence, other wave functions with a primary wave vector $\vec{K}'$, such that $\vec{K}'_{||}+\vec{G}_{||}=\vec{K}_{||}$, can couple out to the same external state as $e^{-i\vec{K}\cdot\vec{r}}$ through its secondary components. Mahan called this "secondary-cone emission." The states through which secondary-cone emission can occur are just those states which appear along lines of equal $\vec{k}_{||}$ in the *reduced-zone* scheme. We see, then, that the extended-zone scheme works well if primary-cone emission dominates secondary-cone emission; otherwise, the reduced-zone picture is appropriate and interpretation of the ARPES results becomes very difficult.

The ratio of secondary to primary components in a free-electron-like wave function is usually small. In addition, a recent calculation by Chiang *et al.*[17] demonstrates a mechanism for the suppression of the secondary-cone emission. They propose that the transmission of electrons through the surface depends not only on the rigorous matching of $\vec{k}_{||}$, but also upon a rough matching of $\vec{k}_\perp$ as well. This latter dependence reflects the need for substantial local overlap between the internal and external wave functions, rather than any requirements of the long-range periodicity of the crystal perpendicular to the surface. Plane waves outside the crystal, with perpendicular wave vector $\vec{k}_{\perp o}$ couple most strongly with internal states with $\vec{k}_{\perp i}$ such that $(\hbar\vec{k}_{\perp i})^2+2mE_0=(\hbar\vec{k}_{\perp o})^2$. Chiang *et al.* demonstrate that this criterion is satisfied best by the primary-cone final states for GaAs. They did this by calculating the perpendicular Fourier components of the final states calculated by Pandey[6] with the nonlocal pseudopotential method. They demonstrate that almost all of the intensity in the $\vec{k}_\perp$-matching Fourier components originates in the primary-cone emission bands. (See Fig. 1, Ref. 42.)

In the usual one-electron band-structure calculations, the crystal potential in CdS opens up substantial gaps in the final-state bands at zone boundaries. Yet, the final-state bands in our ARPES studies have the parabolic shape characteristic of free-electron materials. There is no substantial attenuation of the photoemission intensity at the zone boundaries, though the photoemission peaks may change abruptly as the energy is varied through one of these regions.

The occurrence of photoemission into band gaps was noted in some of the earliest ARPES work on clean single crystals. Band-gap emission is usually attributed to transitions directly to surface-evanescent final states. These are states with complex wave vectors along the surface normal, which form the only solutions to the bulk Schrödinger equation in the energy gaps. Emission through surface-evanescent states is outside the realm of the three-step model, as traditionally articulated, since complex wave vectors cannot be conserved between the initial and final states of the optical transition. Furthermore, since the weakly penetrating surface-evanescent final states simply do not overlap as many initial states, the surface-evanescent emission would be weaker than emission through bulk Bloch states.

A discussion of the nature of the final states is presented by Jepsen *et al.* in a very recent paper.[49] With the use of detailed single-step calculations they predict the intensities and line shapes, in addition to the energy positions, of features in the ARPES data on Ni(110) and Cu(110). We shall emphasize general results of their model that might be applicable to the present study. Their work involved calculations of the dipole transition rates from the initial states to "time-reversed LEED" final-state wave functions.[50] The latter states consist of plane waves propagating toward the ARPES detector outside the crystal matched onto bulk and surface-evanescent states at the crystal surface. The critical feature of this model is that the Schrödinger equation is solved using a crystal potential with an imaginary part $i\beta(E)$ that imposes an energy-dependent damping on all wave functions. This damping reproduces the effects of inelastic electron scattering, but it also has dramatic effects on the form of the final-state bands. (See Fig. 1, Ref. 49.) Without damping, the eigenstate wave vectors become complex only in the energy gaps. With finite damping, the wave vectors at all energies have an imaginary component. As a result, the

penetration depth of the LEED final states is more nearly uniform at all energies, regardless of the presence of gaps. Therefore, the bandgap emission is not necessarily weaker than that which takes place through the damped bulklike states. The real part of the band dispersions is also substantially modified by inclusion of the damping term in the crystal potential. The appearance of gaps is, of course, a consequence of interference of waves scattered from the periodic crystal potential. Damping causes localization of the final states, effectively preventing long-range interference. Jepsen *et al.* demonstrate how the gaps in the Ni and Cu band structures are actually removed by the introduction of damping. Away from the zone boundaries, the final-state bands calculated without damping are near the real parts of the bands calculated with damping. Near the gaps, damping changes the real part of the dispersion back toward the free-electron dispersions. (Note that the real part of the wave vector is the part that is important for the $\vec{k}_\perp$-matching model of Chiang *et al.*) An extension of this model to CdS would explain the results we obtain.

The sophisticated one-step photoemission calculations mentioned above are required to fully explain the intensities and line shapes obtained in ARPES. However, by employing damped final-state bands the accuracy of the three-step model could apparently be enhanced while maintaining its intrinsic simplicity and its usefulness as an intuitive model of the photoemission process. Our results suggest that such an approach might have wide-ranging applicability.

C. Surface states

We have ignored the effects of surface-state emission in the foregoing discussion of the angle-resolved results. This is justified by a number of considerations. Since surface states are localized along the perpendicular coordinate, they may disperse with $\vec{k}_{||}$, but they will not demonstrate any dispersion with $\vec{k}_\perp$. Any features that show dispersion are, therefore, clearly not surface states. All of the ARPES features used in the determination of the bulk band structure which appear in more than a few consecutive CFS spectra show finite dispersion. Contamination tests also support our conclusions. Surface states are a product of, and so are sensitive to, the exact potential at the surface. Contamination of the surface alters this potential and removes or redistributes the surface states. As a check for surface states, both cleavage faces of CdS were deliberately exposed to 10^5 L (1 L=langmuir=10^{-6} Torr sec) of room air after a series of spectra had been completed. After the exposure, photoelectron spectra were selectively retaken over a range of energies and angles. A 0.1-eV decrease in the work function resulted from the contamination, but only slight changes in the photoelectron spectra were observed. We take this as an indication that the primary source of emission is bulk electronic states, at least at the photon energies employed in the contamination tests, $\hbar\omega < 32$ eV.

The lack of surface-state emission in our spectra is consistent with the predictions of the only theoretical calculations for the surface electronic structure of a II-VI—compound wurtzite semiconductor. These were performed by Ivanov and Pollman[51] for ZnO using the tight-binding approach. Note that all spectra in this study have $\vec{k}_{||}$ along $\Gamma X'$ in the surface reciprocal lattice. ($\Gamma X'$ is along the c axis for both surfaces: See Ref. 51 for a complete description of the geometry of the surface Brillouin zones.) The calculations predict that there are no surface states or resonances along this line for the $(11\bar{2}0)$ surface. Two surface resonances and one surface state occur along $\Gamma X'$ for the $(10\bar{1}0)$ surface. The lone surface state is found at point X' and is mostly composed of bonding p orbitals oriented along the c axis. It should, therefore, be seen only in the $\vec{E}||\vec{c}$ spectra with $\vec{k}_{||}=\vec{k}_{\Gamma\Delta A}$.

The lack of surface states in ZnO (Ref. 50) is attributed to the ionic nature of this compound. Cleaving in ionic materials results in less charge redistribution than in covalent semiconductors since covalent bonds are not broken and dangling bonds are not created. ZnO is slightly more ionic than CdS,[52] but the surface states of both materials should be similar.

VI. FINE STRUCTURE OF THE Cd 4*d* LEVELS

The cation d levels of II-VI compounds are bound by about 9 eV less than those of the III-V compounds. As a consequence these d levels fall between the chalcogen derived s and p valence bands. The III-V cation d states can be accurately treated as isolated, quasiatomic core levels. However, this is not necessarily true for II-VI compounds. We find that in the II-VI compounds these states may exhibit additional splitting above and beyond the normal d-level spin-orbit splitting. We interpret this as evidence for hybridization effects and/or itinerant behavior, although a detailed explanation of the core-level shape is not yet available. Hybridization of the Cd 4*d* levels with the S 3*s* states has been predicted on theoretical grounds.[7] Himpsel *et al.*[53] have observed 0.17-eV dispersion for the 3*d* levels of metallic zinc, but direct evidence for delocalized d levels in II-VI compounds has not been reported.

Several authors have called attention to the differences between the angle-integrated photoelectron spectra of the Cd 4*d* levels in metallic Cd and in the cadmium chalcogenides.[13,15] (See Fig. 7, curves *a* and *b*). Metallic Cd exhibits two well-resolved Cd 4*d* peaks with an apparent spin-orbit splitting of approximately 0.9 eV compared to the atomic splitting of 0.79 eV.[54] In CdS these peaks move to a splitting of 0.6 or 0.7 eV and become broadened and unresolvable. At some photon energies, an additional weak shoulder is observed on the low-binding-energy side of the 4*d* levels. Cubic CdTe,[12,15] and to a lesser extent CdSe,[13] exhibit a similar angle-integrated Cd 4*d* spectrum, but the shoulder is *not* present in the 3*d* spectra of zinc chalcogenides.[12] The present results provide new insight into the source of this feature. We find that the weak shoulder can be resolved as a strong, distinct peak in the ARPES spectra with certain choices of energy, polarization, and emission direction. Moreover, these parameters affect the peak positions and intensities of the entire 4*d* manifold.

These effects are clearly seen in Fig. 7. Higher energy resolution (0.15 eV) was used to record the Cd 4*d* spectra

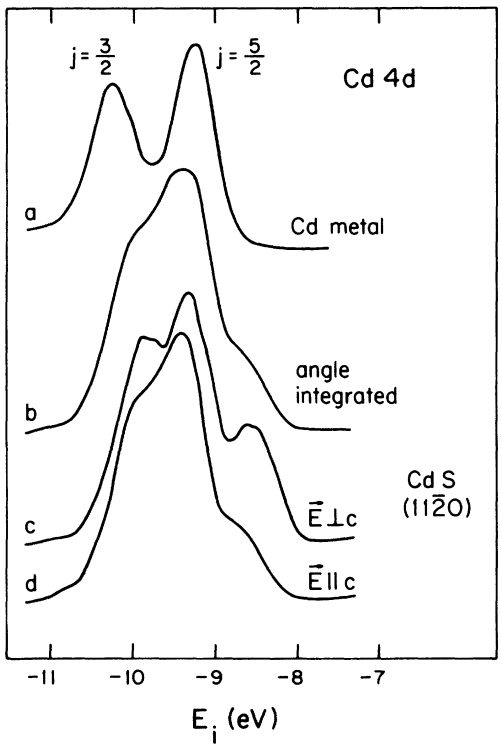

FIG. 7. Comparison of four Cd 4*d* core-level photoelectron spectra obtained under different conditions. Curve *a* is an EDC of the spin-orbit-split Cd 4*d* level of metallic cadmium ($\hbar\omega = 40.8$ eV, from Ref. 30). Shapes of the Cd 4*d* spectra of CdS are quite different, as is apparent in curves *b*–*d*, which are taken on CdS(11$\bar{2}$0). Curve *b* is an angle-integrated EDC, $\hbar\omega = 40$ eV, and $\vec{E}\perp\vec{c}$. Angle-resolved normal-emission CFS spectra, curves *c* and *d*, demonstrate the polarization dependence of the Cd 4*d* emission. In particular, the low-binding-energy shoulder, which is seen in *b* and *d*, can be resolved as a distinct peak in *c*.

in both polarizations in Fig. 7, curves *c* and *d*. These spectra were taken in the normal-emission CFS mode from the (11$\bar{2}$0) surface. With $\vec{E}\perp\vec{c}$, the low-binding-energy shoulder accounts for 15–20% of the peak area in Fig. 7(d). The shoulder is also intense for similar spectra with $\vec{k}_{\parallel} = \pm\vec{k}_{\Gamma A\Gamma}$, suggesting that it might be associated with band-structure effects. The energy and direction, for which the low-binding-energy emission is most intense, have already been associated above with the *K* point. Surface defects or surface shifts like those recently discovered for other semiconductor surfaces[55] cannot account for the shoulder. The surface sensitivity at the energies employed in our study is too low to emphasize surface features. Furthermore, soft-x-ray photoelectron spectra, which have higher surface sensitivity, do not show any enhancement of the low-binding-energy feature.

Crystal-field-splitting effects are undoubtedly important for states as shallow and spatially extended as the Cd 4*d* levels. However, crystal-field splitting by itself is not sufficient to explain our data. The observed Cd 4*d* line shape is incompatible with simple models of 4*d* crystal-field splitting, which neglect hybridization effects. For example, Ley *et al.*[14] show that the atomic 4*d* doublet can split into three peaks under tetrahedral crystal fields. But the ordering, energy splittings, and relative populations of the peaks predicted by their model do not coincide with the three peaks that we observe.

In Fig. 8, a series of Cd 4*d* spectra are shown for both polarizations. We find no direct evidence for dispersion in these spectra, but our data do not rule out itinerant nature for these states. Because of intrinsic broadening and the large number of bands, significant dispersion might go undetected in the ARPES spectra. The total width of the 4*d* band is about 1.2 eV, exclusive of lifetime-broadening effects. The width of the 4*d* band increases from atom to metal to covalent solid. This leads us to look to the Cd–S bonding for explanations of the behavior of the Cd 4*d* spectra in CdS. If the 4*d* states are nonlocalized, it is necessary to postulate some interaction with sulfur states to account for the itinerant behavior of the 4*d* states, since the Cd-Cd nearest-neighbor distance is too large to support direct overlap. Hybridization of the Cd 4*d* and S 3*s* states has been suggested in theoretical studies of zinc-blende CdS.[7] However, the wurtzite structure, with 36 loosely bound electrons per unit cell, may be too complicated to allow fully realistic calculations of this interaction.

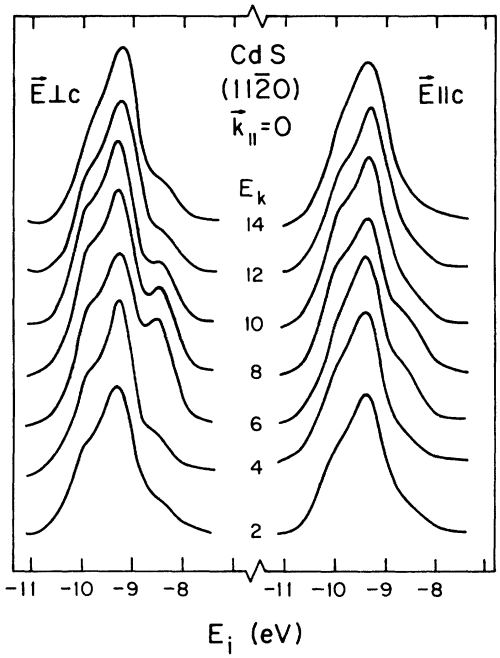

FIG. 8. Two series of normal-emission CFS spectra of the Cd 4*d* states taken with orthogonal orientations of the polarization vector. Note that the low-binding-energy shoulder is enhanced for $\vec{E}\perp\vec{c}$ polarization and kinetic energies near 8 eV. Since the main Cd 4*d* spectral features are not similarly enhanced, we presume that the shoulder emission arises from states of quite different symmetry than the main photoelectron peaks. These states apparently couple well to the *K*-like final states, which occur near 8-eV kinetic energies. Electronic structure of the Cd 4*d* states has never been calculated in wurtzite CdS.

VII. CONCLUSIONS

We have performed an angle-resolved photoemission study of the electronic structure of wurtzite CdS using synchrotron radiation. Our study indicates the presence of substantial shortcomings in the current theoretical description of the electronic structure of wurtzite CdS. The most prominent of these are the underestimation of the width of the S $3p$–derived valence bands and the inadequate treatment of the Cd $4d$ core levels. Significant advances have been made in band-structure calculation techniques since the above-mentioned studies were published. We provide a number of new critical points in the valence bands to guide new calculations. In light of the fundamental questions raised by our data and the technological importance of this material, we feel that a theoretical review of the band structure of wurtzite CdS is overdue.

The Cd chalcogenides show broadening of their Cd $4d$ levels. This work provides the first angle-resolved study of this effect, and shows it to be a richer phenomenon than was previously supposed. Any calculations that can explain our observations will undoubtedly improve our understanding of the influence that shallow d states exert on the overall electronic structure of materials involving group-II elements.

Calculations of the conduction bands to higher energies, possibly including damping, would provide a check on our assumptions about the $\vec{k}$ vectors of final states, and would facilitate further studies. Furthermore, band-structure calculations for our final-state range would be needed to interpolate the bands between the high-symmetry points.

By investigating a wurtzite II-VI compounds we also tested the applicability of ARPES techniques for three-dimensional band-structure mapping in a new class of materials. Successful band-structure mapping has been restricted primarily to three classes of systems: Quasi-two-dimensional systems such as layered compounds or overlayers for which $\vec{k}_\perp$ conservation is not very important or metal or zinc-blende semiconductors that have relatively small, simple unit cells and free-electron-like final states. The extension of ARPES techniques to other materials requires a thorough understanding of the photoemission process. This study reinforces some of the recently developed ideas about the nature of the final states that are important in photoemission. We are encouraged that ARPES can be adapted to study the band structure of many other compounds, especially with support from the theoretical side. There are several factors that were crucial for achieving the results we have presented: Qualitatively accurate initial-state band-structure calculations, access to polarized, tunable synchrotron radiation, and the ability to take CFS spectra, particularly in the off-normal emission geometry.

ACKNOWLEDGMENTS

The author acknowledges helpful discussions with G. Margaritondo and M. M. Traum concerning these experiments. Technical assistance provided by the staff of the University of Wisconsin Synchrotron Radiation Center is greatly appreciated. The center is supported by the National Science Foundation under Grant No. DMR-74-15089. This work is supported in part by the National Science Foundation under Grant Nos. DMR-78-22205 and DMR-82-00518.

[1]For a review of the technological importance of CdS and other II-VI compounds, see A. N. Georgobiani, Usp. Fiz. Nauk. 13, 129 (1974) [Sov. Phys.—Usp. 17, 424 (1974)].

[2]J. C. Phillips, Phys. Rev. 133, A452 (1964).

[3]M. Cardona and G. Harbeke, Phys. Rev. 137, A1467 (1965).

[4]R. Baumert and J. Gutowski, Phys. Status Solidi B 107, 707 (1981).

[5]J. R. Chelikowski and M. L. Cohen, Phys. Rev. B 14, 556 (1976).

[6]K. C. Pandey and J. C. Phillips, Phys. Rev. B 9, 1552 (1974).

[7]A. Zunger and A. J. Freeman, Phys. Rev. B 17, 4850 (1978).

[8]D. J. Stuckel, R. N. Euwema, T. C. Collins, F. Herman, and R. L. Kortrum, Phys. Rev. 179, 740 (1969).

[9]S. I. Kurganskii, O. V. Faberovich, E. P. Domashevskaya, Fiz. Tekh. Poluprovodn. 14, 1315 (1980) [Sov. Phys.—Semicond. 14, 775 (1980)].

[10]D. B. Holt, Thin Solid Films 24, 1 (1974).

[11]M. A. Mojumder, Solid State Commun. 43, 13 (1982).

[12]D. E. Eastman, W. D. Grobman, J. L. Freeouf, and M. Erbudak Phys. Rev. B 9, 3480 (1974).

[13]C. F. Brucker and L. J. Brillson, J. Vac. Sci. Technol. 18, 787 (1981).

[14]L. Ley, R. A. Pollak, F. R. McFeely, S. P. Kowalczyk, and D. A. Shirley, Phys. Rev. B 9, 600 (1974).

[15]N. J. Shevchik, J. Tejeda, D. W. Langer, and M. Cardona, Phys. Status Solidi 60 (1973).

[16]N. V. Smith, in *Photoemission in Solids, Part I,* Vol. 26 of *Topics in Applied Physics,* edited by M. Cardona and L. Ley (Springer, Berlin, 1978), p. 237.

[17]T. C. Chiang, J. A. Knapp, M. Aono, and D. E. Eastman, Phys. Rev. B 21, 3513 (1980).

[18]T. C. Chiang and D. E. Eastman, Phys. Rev. B 22, 2940 (1980).

[19]For a study of the surface states on zinc-blende ZnSe, see A. Ebina, T. Unno, Y. Suda, H. Koinuma, and T. Takahashi, J. Vac. Sci. Technol. 19, 310 (1981). For a study of the surface states of wurtzite ZnO, see W. Göpel, J. Pollmann, I. Ivanov, and B. Reihl, Phys. Rev. B 26, 3144 (1982).

[20]R. N. Euwema, T. C. Collins, D. G. Shankland, and J. S. DeWitt, Phys. Rev. 162, 710 (1967).

[21]T. K. Bergstresser and M. L. Cohen, Phys. Rev. 164, 1069 (1967).

[22]The 1-Ω-cm CdS samples were supplied by Cleveland Crystals, Inc. They were n type ($n=10^{16}$ cm^{-3}) due to excess Cd.

[23]N. G. Stoffel and G. Margaritondo, Rev. Sci. Instrum. 53, 18 (1982).

[24]G. J. Lapeyre, R. J. Smith and J. Anderson, J. Vac. Sci. Technol. 14, 384 (1977).

[25]E. I. Rashba, Fiz. Tverd. Tela (Leningrad) 1, 407 (1959) [Sov. Phys.—Solid State 1, 368 (1959)].

[26]E. P. Domashevskaya, V. A. Terekhov, L. N. Marshakova, Ya. A. Ugai, V. I. Nefedov, and N. P. Sergushin, J. Electron. Spectrosc. Relat. Phenom. 9, 261 (1976).
[27]T. Grandke, in *Festkörperprobleme XIX* (Viewig, Braunschweig, 1979).
[28]Y. Petroff and P. Thiry, Appl. Opt. 19, 3957 (1980).
[29]F. J. Himpsel, Appl. Opt. 19, 3964 (1980).
[30]J. Stohr, P. S. Wehner, R. S. Williams, G. Apai, and D. A. Shirley, Phys. Rev. B 17, 587 (1978).
[31]P. Thiry, D. Chandesris, J. Lecante, C. Guillot, R. Pinchaux, and Y. Petroff, Phys. Rev. Lett. 43, 82 (1979).
[32]J. A. Knapp, F. J. Himpsel, and D. E. Eastman, Phys. Rev. B 19, 4952 (1979).
[33]W. Eberhardt and E. W. Plummer, Phys. Rev. B 21, 3245 (1980).
[34]D. E. Eastman, F. J. Himpsel, and J. A. Knapp, Phys. Rev. Lett. 44, 95 (1980).
[35]F. J. Himpsel and D. E. Eastman, Phys. Rev. B 18, 5236 (1978).
[36]P. Heimann, H. Miosga, and H. Neddermeyer, Solid State Commun. 29, 463 (1980).
[37]W. E. Spicer, Phys. Rev. 112, 114 (1958).
[38]E. O. Kane, Phys. Rev. Lett. 12, 97 (1964); H. Y. Fan, Phys. Rev. 68, 43 (1945); L. Apker, E. Taft, and J. Dickey, Phys. Rev. 74, 1462 (1948).
[39]T. Grandke, L. Ley, and M. Cardona, Phys. Rev. B 18, 3847 (1978).
[40]J. Hermanson, Solid State Commun. 22, 9 (1977).
[41]E. Dietz and D. E. Eastman, Phys. Rev. Lett. 41, 1674 (1978).
[42]J. R. Chelikowsky, Solid State Commun. 22, 351 (1977).
[43]S. Bloom and I. Ortenburger, Phys. Status Solidi B 58, 561 (1973); S. Bloom, J. Chem. Phys. Solids 32, 2027 (1970); D. Jones and A. H. Lettington, Solid State Commun. 11, 701 (1972).
[44]N. G. Stoffel, Ph.D. thesis, University of Wisconsin, 1983, University Microfilms International (unpublished).
[45]W. K. Kohn and L. J. Sham, Phys. Rev. 140, A1133 (1965).
[46]R. N. Euwema, D. J. Stuckel, and T. C. Collins, in *Proceedings of the Conference on Computational Methods in Band Theory* (Plenum, New York, 1971), p. 82.
[47]P. V. Smith, J. Phys. Chem. Solids 37, 589 (1976).
[48]G. D. Mahan, Phys. Rev. B 2, 4334 (1970).
[49]D. W. Jepsen, F. J. Himpsel, and D. E. Eastman, Phys. Rev. B 26, 4039 (1982).
[50]P. J. Feibelman and D. E. Eastman, Phys. Rev. B 10, 4932 (1974).
[51]I. Ivanov and J. Pollman, Phys. Rev. B 24, 7275 (1981).
[52]J. C. Phillips, *Bonds and Bands in Semiconductors* (Academic, New York, 1973).
[53]F. J. Himpsel, D. E. Eastman, E. E. Koch, and A. R. Williams, Phys. Rev. B 22, 4604 (1980).
[54]F. Herman and S. Skillman, *Atomic Energy Levels* (Prentice-Hall, Englewood Cliffs, New Jersey, 1963).
[55]D. E. Eastman, T. C. Chiang, P. Heimann, and F. J. Himpsel, Phys. Rev. Lett. 45, 656 (1980); 45, 112 (1980).